Research Article Vol. 36, No. 8 / August 2019 / Journal of the Optical Society of America B 2013

Journal of the Optical Society of America B

OPTICAL PHYSICS

Superchannel engineering of microcombs for optical communications

Óskar B. Helgason,[1,*] Attila Fülöp,[1] Jochen Schröder,[1] Peter A. Andrekson,[1] Andrew M. Weiner,[2] and Victor Torres-Company[1]

[1]Department of Microtechnology and Nanoscience, Chalmers University of Technology, Gothenburg, Sweden
[2]School of Electrical and Computer Engineering, Purdue University, West Lafayette, Indiana 47907, USA
*Corresponding author: skarb@chalmers.se

Received 29 March 2019; revised 5 June 2019; accepted 5 June 2019; posted 10 June 2019 (Doc. ID 363790); published 9 July 2019

Microresonator frequency combs (microcombs) are a promising technology for generating frequency carriers for wavelength division multiplexing (WDM) systems. Multi-terabit per second WDM coherent transmitters have recently been demonstrated using both dissipative Kerr solitons and mode-locked dark pulses in optical microresonators. These experiments have focused on microcombs designed to cover a large portion of the erbium-doped fiber window. However, the question of optimum bandwidth for microcombs in WDM systems has not been addressed. Here we show that segmenting the bandwidth into smaller microcomb-driven superchannels results in an improvement of power per line. Through numerical simulations we establish a quantitative comparison between dark-pulse and soliton microcombs in WDM systems, including aspects such as conversion efficiency, tolerance to intrinsic cavity loss, and group velocity dispersion engineering. We show that the improvement of minimum line power scales linearly with the number of superchannels for both types of microcombs. This work provides useful guidelines for the design of multi-terabit per second microcomb-based superchannel systems.

https://doi.org/10.1364/JOSAB.36.002013

1. INTRODUCTION

Over the last decade, microresonator combs (or microcombs) have attracted growing attention in the research community [1,2]. They are a chip-scale solution, employing the Kerr effect to generate equally spaced, coherent lines in the frequency domain [3,4]. The small cavity dimensions allow the line spacing of the combs to be orders of magnitude larger than what can be obtained with standard passively mode-locked lasers. These qualities, along with the potential for hybrid integration [5–8], justify the interest of microcombs for several applications [3]. Each application has different requirements in terms of bandwidth, power per line, and line spacing. For instance, self-referencing requires coherent octave-spanning bandwidth and sufficient line spacing stability [9]. In contrast, telecommunications require a few terahertz (THz) of bandwidth, lines with low linewidth, and high conversion efficiency (i.e., the fraction of pump power converted to other comb lines) in order to reach sufficiently high power per line and optical signal-to-noise ratio (OSNR) [10–12].

Microcombs have been demonstrated as carrier generators for wavelength division multiplexing (WDM) transmission links [10,13–18]. The findings in Ref. [17] showed that a pump laser of narrow linewidth is advantageous toward higher data rates. The experiment in Ref. [15] used a microcomb having a dissipative Kerr soliton [19] circulating in the cavity (henceforth soliton microcomb). Two microcombs pumped with high-power lasers were interleaved to generate a large number of lines covering the C and L optical telecommunication bands. A series of transmission experiments were conducted, resulting in data rates reaching 50 Tb/s using both QPSK and 16QAM modulation formats, depending on individual comb line power. In Ref. [10], a mode-locked dark-pulse Kerr comb (henceforth dark-pulse microcomb) [20] was used to generate carriers in the C band with sufficient optical OSNR per WDM channel to achieve 64QAM modulation and 4.4 Tb/s data rates.

Even more complex modulation formats or higher data rates could be achieved with further optimization of the microcombs in terms of line power. Starting with a microcomb with sufficiently high power is critical to overcome the losses in an integrated transmitter and attain the necessary OSNR per WDM channel [10]. This is true regardless of whether the microcomb sustains a dark pulse or a soliton state. However, it is so far not clear which of these two coherent states would be more desirable for WDM transmission experiments.

In the past years, the system dynamics of microcombs have been rigorously investigated for both soliton [19,21–26] and dark-pulse microcombs [20,23,27–31]. Having a simple

temporal structure, an intracavity solution for the amplitude of dissipative Kerr solitons has been derived [19,32]. In contrast, mode-locked dark pulses have a more complicated temporal structure, for which an analytical solution has not been fully determined. The circulating waveform consists of a bright background with a dip that contains ripples at the bottom [20,29], which can be described as an interlock between switching waves connecting the homogeneous steady-state solutions of the bistability curve in the cavity [33]. This waveform is relevant for practical applications because it offers a superior conversion efficiency compared to dissipative Kerr solitons, which promises a higher power per line [27].

The closed-form solution of dissipative Kerr solitons has been used to predict the scaling of the generated comb lines in terms of bandwidth and power per line [21,22]. The investigation in [21] shows that the average power per line scales linearly with the laser input power and inverse quadratically with the number of lines generated. This implies that employing soliton microcombs generating a lower number of lines would be substantially beneficial from the perspective of improving the overall conversion efficiency.

Here, instead of producing a large number of lines with a single microcomb, we suggest to segment the WDM bandwidth into superchannels, each driven by a narrower microcomb. A superchannel contains a group of channels that are modulated with high spectral efficiency in the same place, routed together through the same optical path and received together at the same destination [34,35]. This WDM architecture segments the transmission spectrum into multiple superchannels. The superchannels are treated as separate entities in the optical network, where each could be fed by a narrow microcomb.

Assuming that a single microcomb is replaced by M narrower combs while keeping the same total optical power, this approach suggests that the performance in terms of power per line can be improved by a factor M (see Fig. 1). At the same time, by lowering the power from each laser, this approach becomes more suitable for hybrid integration [5]. We show, through numerical simulations, that soliton and dark-pulse microcombs both benefit from segmenting the available bandwidth into narrower superchannels. We show that the scaling of power per line derived in Ref. [21] for dissipative Kerr solitons also applies for mode-locked dark pulses. Part of this work was presented in Ref. [36]. Here, we provide a more in-depth study quantifying the impact of losses and nonlinearity, and we discuss the scaling laws with the group velocity dispersion (GVD) and conversion efficiency. Furthermore, we investigate the practical feasibility of the microcombs with state-of-the-art silicon nitride technology.

The work is structured as follows. In Section 2, we present in detail the scaling laws of the superchannel arrangement. The third section is devoted to numerical simulations that verify the scaling laws from Section 2 and their dependence with intrinsic losses, GVD, and conversion efficiency. Section 4 analyzes the implications and challenges of dealing with narrower combs with regards to waveguide designs based on silicon nitride.

2. SCALING OF MICROCOMB-DRIVEN SUPERCHANNELS

A basic requirement for microcombs in optical communications is to generate sufficient power per line to enable the desired modulation format. In most WDM experiments the comb lines are equalized to the line with the lowest power P_{min} in order to ensure even performance across the superchannel [10]. To optimize this minimum line power, it is important to recognize the performance scaling of microcombs. The conversion efficiency and the 3-dB bandwidth can be deduced from the temporal field of the soliton [21,22], leading to the scaling equation for the average power per line. Using a similar approach, the scaling of the minimum line power is described as

$$P_{\mathrm{min}} = K \cdot \frac{\theta^2}{(\alpha_{\mathrm{i}} L + \theta)^2} \cdot \frac{P_{\mathrm{in}}}{N^2}, \tag{1}$$

where θ is the power coupling coefficient between resonator and bus waveguide, L is the cavity length, α_{i} is the absorption per unit length in the cavity, and P_{in} is the power of the pump laser. N is the number of generated lines within a certain bandwidth. The value of the proportionality factor K depends on the exact cutoff bandwidth. For an overcoupled cavity, this equation will mostly depend on the input power and number of lines ($P_{\mathrm{min}} \approx K \cdot P_{\mathrm{in}}/N^2$).

Let us now compare two comb cases providing N carriers over the C and L bands using P_0 total optical power (see Fig. 1). The first case is a single comb pumped with optical power $P_1 = P_0$ generating $N_1 = N$ lines. In the second case the

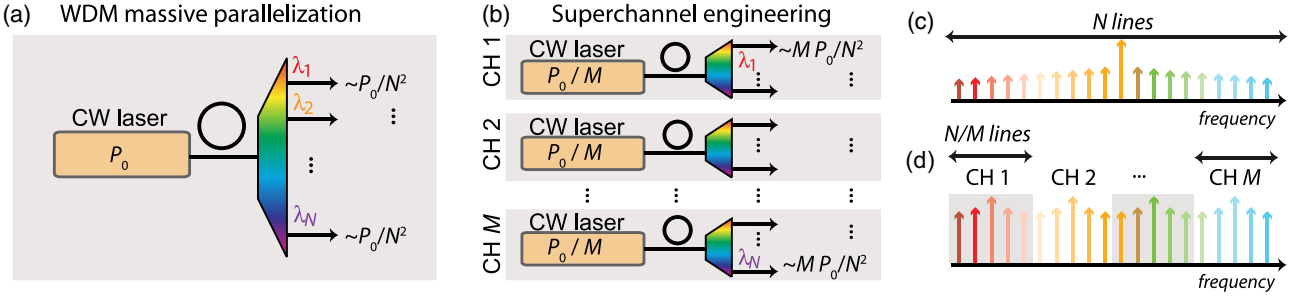

Fig. 1. Diagram in (a) shows a basic layout where a single microcomb source provides all lines for a WDM system. In comparison, the diagram in (b) shows how the same number of lines can be provided using narrower microcombs in an arrangement of M superchannels. The sketches in (c) and (d) show the combined comb spectra of the systems in (a) and (b), respectively, before equalization of line power. The system in (b) is expected to have M times higher power per line than the system in (a), while still using the same total optical input power.

frequency band has been segmented in M superchannels, each providing $N_2 = N/M$ lines while being pumped with optical power $P_2 = P_0/M$. According to the overcoupled version of Eq. (1), one can approximate the power per line in cases 1 and 2 as $P_{\mathrm{min}1} \propto P_1/N_1^2 = P_0/N^2$ and $P_{\mathrm{min}2} \propto P_2/N_2^2 = M \cdot P_0/N^2$, respectively. This indicates M times higher power per line for the case where the available bandwidth is distributed in M superchannels. Hence, there is a trade-off between integration complexity and power efficiency, which can be balanced in different ways. Filling up the C band with a channel spacing of 100 GHz with a single microcomb would require 44 lines. Decreasing the line spacing to 50 GHz would result in 4 times higher pump power to maintain the same power per line. If instead one chose to segment the bandwidth in four superchannels, each driven by a 50 GHz microcomb (each with 22 lines), the power required to drive each microcomb would decreased by a factor of 4, but at the expense of quadrupling the number of pump lasers. The optimum number of lines per superchannel will depend on the specifics of the communication system, and it would therefore have to be determined on a case-by-case basis. For example, in Ref. [37] the power savings due to the simplification of digital signal processing will saturate when applied to over ten lines, whereas in Ref. [15] the authors reported power consumption that decreases considerably with the number of comb lines.

It is important to note that the derivation above relies on scaling laws that have been derived only for soliton microcombs. However, in the next section we verify and numerically demonstrate that the same scaling applies for the minimum line power of dark-pulse microcombs.

3. OPTIMIZED PERFORMANCE OF DISSIPATIVE KERR SOLITONS AND MODE-LOCKED DARK PULSES IN MICRORESONATORS

To confirm the scaling of the microcomb minimum line power, we implement an optimization process similar to that discussed in Refs. [10,15]. The details of this optimization process are described in the next subsections. After introducing the optimization, we show that both soliton and dark-pulse microcombs display the same scaling as described by Eq. (1). The analysis is followed by an evaluation of the effects of the intrinsic quality factor (Q_i). The bandwidth dependence on GVD is discussed in the subsection after that. In the last subsection, we analyze the origin of the scaling law for dark-pulse microcombs.

A. Optimization Process

For WDM applications, a superchannel should have the same power among the constituent carriers. P_{min} is therefore used as a figure of merit for the optimization process. This assumes that the lines will be equalized to the weakest (lowest power) line within the superchannel bandwidth.

The optimization requires a large collection of stable comb states, each obtained through simulation trials over a parameter space formed by the GVD coefficient (β_2), the coupling coefficient (θ), and the phase detuning between the continuous-wave (CW) pump and the closest resonance (δ_0). With the parameters β_2 and θ being approachable through design and δ_0 being a free parameter within a certain range, P_{min} can be then optimized [10,15]. After acquiring the comb states, we set the desired number of lines and record P_{min}.

A visual example of the optimization process for combs generating 25 lines using 0.25 W input power is displayed in Fig. 2. Numerical values for the simulations are given below. In plots (a) and (b), for soliton and dark-pulse microcombs, respectively, the variation of the figure of merit is displayed as a colormap in terms of β_2 and θ. Note that P_{min} has already been maximized in terms of δ_0 for every pair of β_2 and θ. The highest-performing combs found from the colormaps in (a) and (b) are plotted in (c) and (d). The figures display the outcoupled spectral field, while the inset shows the intracavity waveform. These combs demonstrate an output conversion efficiency (combined power of generated comb lines excluding the pump divided by the input power) of ~0.65 for the dark-pulse microcomb and ~0.16 for the soliton. After equalizing the spectra to the level of P_{min}, the effective conversion efficiency will be ~0.11 for the dark-pulse microcomb and ~0.06 for the soliton. Note also that the optimal microresonators correspond to an overcoupled configuration in both cases. This is consistent with the fact that an overcoupled cavity provides a situation closer to effective critical coupling when the comb losses from the pump perspective are considered [27]. These results indicate that, with proper optimization of the cavity parameters, microcombs with 25 lines featuring powers per line in the order of 1 mW can be achieved for both dark-pulse and soliton microcombs using moderate pump power levels.

One way of improving the conversion efficiency of the soliton microcomb is to increase the number of solitons in the cavity. These states typically consist of multiple solitons whose temporal separation is challenging to fix *a priori* [19,38], resulting in a minimum line power that is lower than that of a single soliton. Another alternative microcomb source that has not yet been introduced, Turing rolls, can be used for WDM transmissions [14]. These structures provide a microcomb with high stability and reproducibility but have a limited number of lines, often with multiple free spectral range (FSR) separation. Because of these challenges, Turing rolls and multi-soliton states are not considered in this study, and the simulations are limited to single solitons and dark pulses.

The simulations were carried out using the split-step method combined with the coupling equations of the resonator [39], solving the system of equations called the Ikeda map [40]. The Ikeda map allows exploration of a broader range of coupling rates than what is possible with the standard Lugiato–Lefever equation. In addition, using this method, the fundamental noise caused by quantum fluctuations can be added to the simulations in a straightforward manner [41]. This allows for a quantitative assessment of the signal-to-noise ratio per line. For a set of parameters, a comb initiation was attempted using an initial temporal field in the cavity, which was a dark square pulse for dark-pulse microcombs [20] and a hyperbolic secant for soliton microcombs [21]. Other states were found by tuning the detuning parameter from already stable comb states. The cavity losses were set to $\alpha_i = 0.1$ dB/cm (equivalent to $Q_i = 3.5 \cdot 10^6$), the free spectral range is FSR = 100 GHz, with a group index $n_g = 2$ and nonlinear coefficient $\gamma = 2\ \mathrm{W}^{-1}\ \mathrm{m}^{-1}$, unless mentioned otherwise.

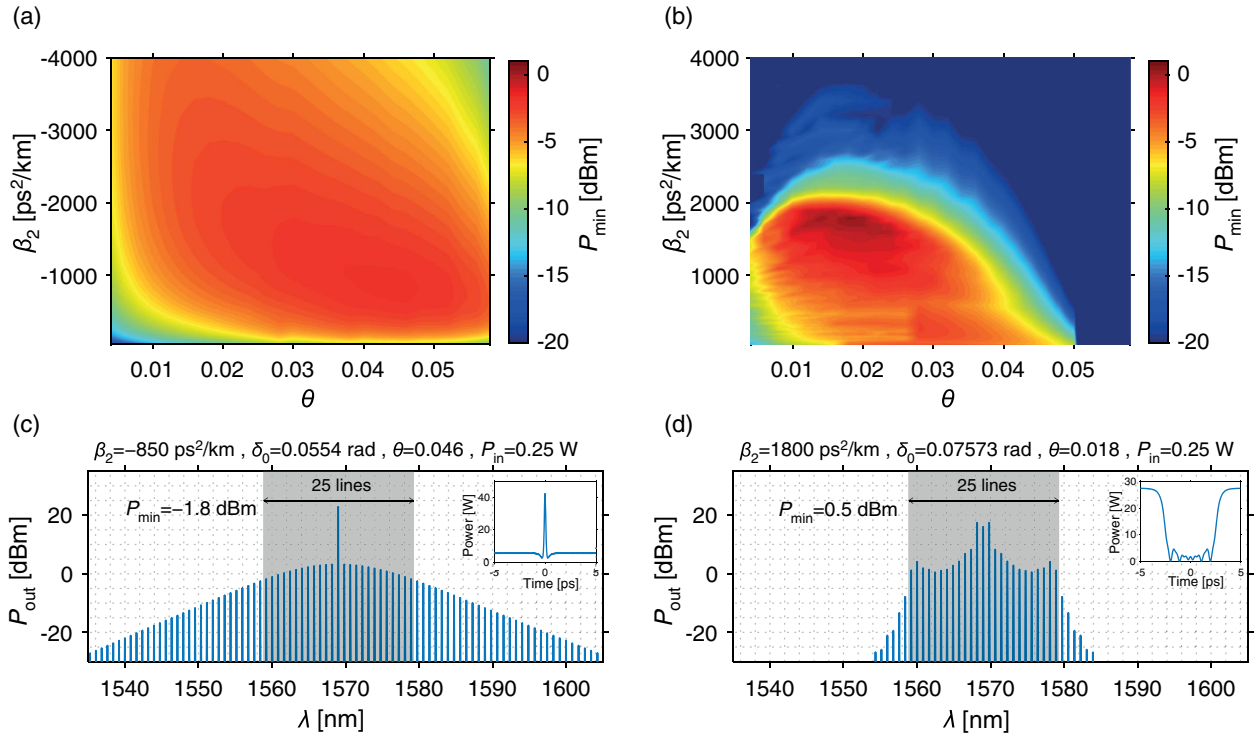

Fig. 2. Example of the optimization process for the generation of a microcomb with fixed number of lines and given pump power (25 and 0.25 W in this case) with 100 GHz spacing. The figures in (a) and (b) show the figure of merit P_{min} as a colormap in terms of β_2 and θ for soliton and dark-pulse microcombs, respectively. The optimization process is tridimensional because it also includes the detuning parameter. The detuning has been chosen such that it maximizes P_{min} for every pair (θ, β_2). The maps show that the figure of merit has a peak value with a relatively small roll-off factor in terms of β_2 and θ. The combs plotted in (c) and (d) correspond to the optima in (a) and (b), respectively. The optical spectra correspond to the outcoupled field, whereas the inset shows the corresponding intracavity temporal power. The set of optimum parameters are explicitly indicated on top of the figures.

These parameters are similar to what can be obtained using silicon nitride microresonators [42–45]. The pump resonance was located close to the middle of the combined C and L bands, i.e., at $\lambda_0 \approx 1569$ nm. All other higher-order effects were neglected.

B. Line Density Scaling and Pump Power Dependence

The aim here is to investigate whether the scaling of P_{min} with input power and number of lines will follow that of Eq. (1). Using the optimization process described in the previous section, we find the highest-performing combs for different input powers and number of lines. Therefore, each of these optimized combs will have a specific GVD, detuning, and coupling value. The results can be found in Figs. 3(a) and 3(b).

The plot in Fig. 3(a) shows that the minimum comb line grows linearly with high pump powers for both dark-pulse and soliton microcombs, which is consistent with Eq. (1) when the cavity is highly overcoupled. The dark-pulse microcombs furthermore deliver roughly 2 dB higher power. *A priori*, this result seems surprising since the conversion efficiency advantage of these microcombs is significantly higher than 2 dB. The reason for this apparent discrepancy is that our figure of merit places a higher emphasis on the minimum line power within the target bandwidth and thus on the smoothness of the spectral envelope. Dark-pulse microcombs display a high spectral structure, and the high conversion efficiency is dominated by the lines closest to the pump, which typically have much higher power than the spectral wings [see Fig. 2(d)]. This is further analyzed in Subsection 3.E.

The plot in Fig. 3(b) displays the relation between the minimum line power and number of lines at two different pump power levels. It shows that the power per line has close to an inverse quadratic scaling with the number of generated lines, both for dark pulse and soliton combs. The plots in (a) and (b) in Fig. 3 therefore demonstrate that optimum combs follow $\sim P_{in}/N^2$ scaling of minimum line power for N generated lines. It indicates that the structure of both dark-pulse and soliton microcombs are affected similarly when scaling the input power, number of lines, and optimization parameters. This supports previous suggestions of mode-locked dark pulses having solitonic dynamics [20,30].

Given that the optimum comb line scales as P_{in}/N^2 for both dark-pulse and soliton microcombs, the superchannel engineering approach in Fig. 1 is valid. As an example, we can compare using a single broad comb generating $N = 101$ lines at $P_{in} = 30$ dBm to 4 superchannels side by side, each generating 25 lines at $P_{in} = 24$ dBm. Using Fig. 3(a) we find $P_{min} = 0.5$ dBm for 25 lines and $P_{min} = -5.5$ dBm for 101 lines for dark-pulse microcombs. Similarly, for soliton microcombs we find $P_{min} = -1.8$ dBm for 25 lines and $P_{min} = -7.9$ dBm for 101 lines. This is an improvement by

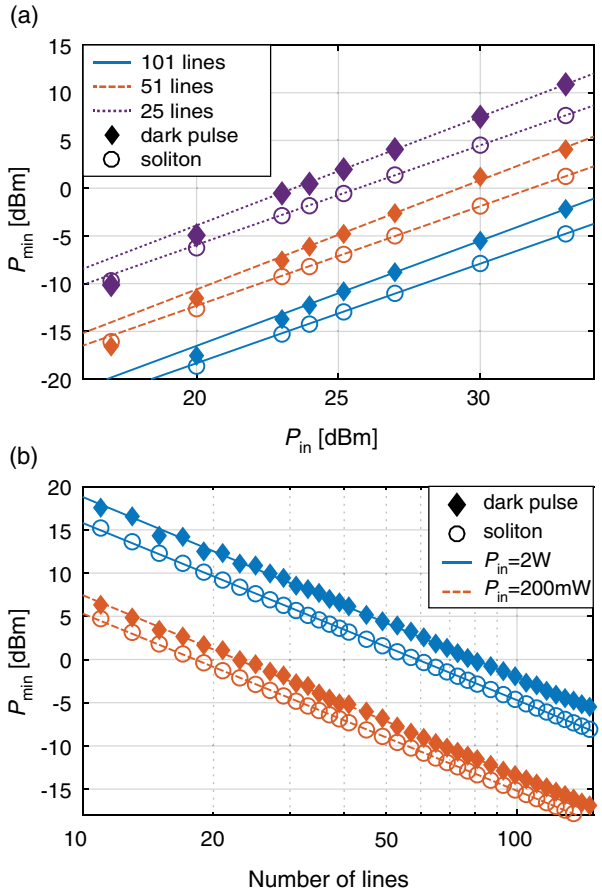

Fig. 3. Plots in (a) and (b) show the optimal combs in terms of power per line found for different input power and number of lines, having 100 GHz spacing. The power per line is described as P_{min}, which is the minimum comb line power. In (a), the data has close to linear behavior for higher input powers, where we draw a linear fit through data points with $P_{in} > 300$ mW. In (b), the power per line scales inverse quadratically with number of lines (~ – 20 dB/decade) when keeping the input power constant. The scaling in (a) and (b) implies that the power per line scales with $\sim P_{in}/N^2$ for both dark-pulse and soliton microcombs.

a factor of 4 in both cases, which complies with the enhancements described in Fig. 1.

C. Interplay between Cavity Losses, Pump Power, and Nonlinearity

The intracavity losses can induce a limitation on the performance of microcombs in terms of minimum line power. In Fig. 4 we show how losses affect the minimum line power by comparing optimized microcombs with intrinsic losses $\alpha_i = 0$ dB/cm ($Q_i \sim \infty$) and $\alpha_i = 0.4$ dB/cm ($Q_i \sim 880000$) for different pump powers. The GVD, detuning, and coupling factor are therefore optimized for both different loss and power levels. The losses decrease the power per line, where the penalty is more severe for lower powers. At low power levels, the required coupling coefficient decreases (roughly as $\theta \propto \sqrt{P_{in}}$), moving the cavity towards the critical coupling condition. This makes the loss contribution in Eq. (1) more significant and therefore decreases the power per line compared to the

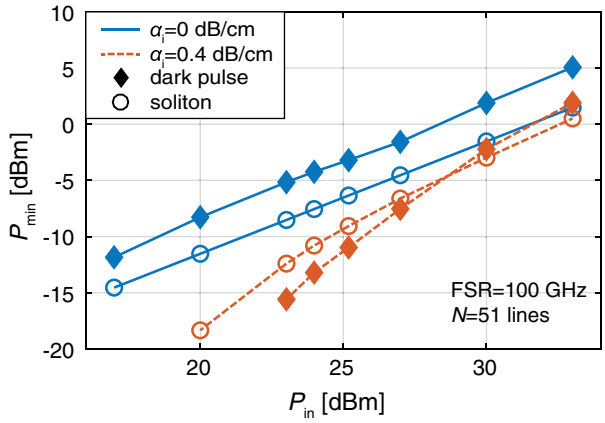

Fig. 4. Dependence of the minimum line power with pump power for different intrinsic losses while generating a fixed number of lines.

highly pumped regime. Dark-pulse microcombs display a more drastic penalty compared to soliton microcombs, which is caused by the optimal coupling being located at lower values. A good example of this is the peak location of the figure of merit in Figs. 2(a) and 2(b), where the optimal coupling for soliton microcombs is in the region $\theta = 0.03$–0.05 but is in the region $\theta = 0.015$–0.025 for dark-pulse microcombs. The optimal dark-pulse microcombs were observed to have a higher-order structure with multiple oscillations at bottom of the pulse. In Ref. [31], these higher-order structures were found to be limited to lower coupling values compared to the soliton space [23] in agreement with our numerical results.

Additionally, we carried out an analysis of the impact of the nonlinear coefficient γ. The results are shown in Fig. 5, where the minimum line power is plotted in terms of the intrinsic Q factor for $\gamma = 2$ W^{-1} m^{-1} and $\gamma = 8$ W^{-1} m^{-1}, with the input power kept constant at 250 mW. The figure shows that the performance in terms of power per line is less affected by the nonlinear coefficient as the intrinsic quality factor is increased. However, when Q_i is lowered, the performance depends more on the nonlinear coefficient. From a superchannel perspective, this observation justifies the efforts in improving the quality

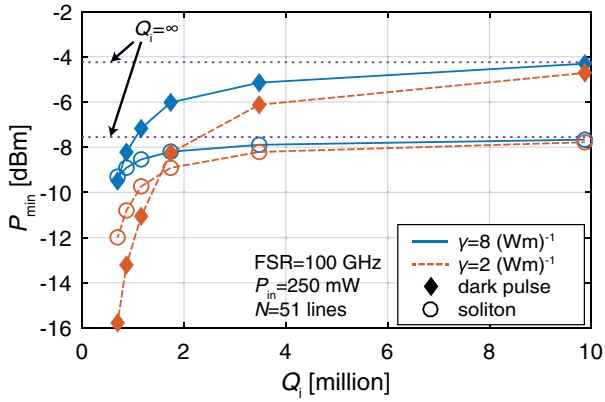

Fig. 5. Dependence of the minimum comb line power with the intrinsic quality factor for different nonlinear coefficients. The dotted line shows the minimum comb-line power as the intrinsic quality factor reaches infinity for both soliton and dark-pulse microcombs.

factor in microresonators [44,45] over alternative platforms that offer a higher nonlinear coefficient at the expense of increased losses.

D. Impact of Group Velocity Dispersion

The GVD is an important parameter when it comes to scaling the number of generated lines [21,46]. In Fig. 6 we display the optimal GVD corresponding to the optimal combs found in Fig. 3(b) as a function of the number of lines. The plot shows a drastic change in dispersion with number of lines, with a clear relation $|\beta_2| \propto 1/N^2$, both for soliton and dark-pulse microcombs. At the same time, the optimum detuning and coupling coefficients were found to be close to constant. Additionally, we observed that the GVD would decrease with higher losses.

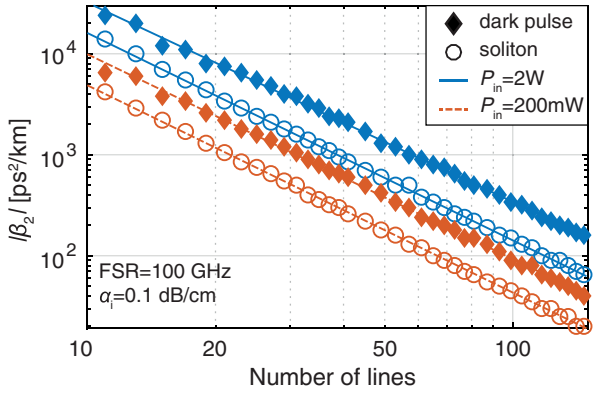

Fig. 6. Dependence of the GVD parameter with number of lines corresponding to the combs in Fig. 3. The trend of the GVD is close to $|\beta_2| \propto 1/N^2$, while the other optimization parameters, θ and δ_0, remain close to constant. The lines are a linear fit to the data points in the log – log space.

While this trend is known for dissipative Kerr solitons [21,46], it has not been discussed for mode-locked dark pulses. For sufficiently narrow microcombs, the required GVD amount becomes extremely high, which, as discussed in Section 4, could be challenging to realize in practice in the case of soliton microcombs.

E. Scaling of Conversion Efficiency

Previously we found that the scaling of P_{min} with the number of lines is $\sim 1/N^2$. Here we investigate what causes this scaling. For soliton microcombs, the conversion efficiency of the pump to all comb lines scales as $\sim 1/N$. Power distribution among generated comb lines thus provides the $\sim 1/N^2$. The scaling of the conversion efficiency for soliton microcombs is well established, since for a fixed FSR, the width of the soliton (and hence the duty factor) scales as $\sim 1/N$ [27]. For mode-locked dark pulses, the explanation for the scaling is less clear. Not only can it be scaled through the GVD like the dissipative Kerr soliton, it can also be tuned into states with different orders of oscillations [31]. This can be described by viewing the dark pulse as the result of two switching waves moving towards each other until their oscillatory tails lock them in place [33]. By changing the detuning, the velocity of these switching waves is changed, manipulating where the oscillatory tails lock together. The width of the dark pulse will increase with the number of oscillations, which leads to a change in conversion efficiency [27]. In order to resolve the contribution from these different effects, we numerically investigate the scaling of conversion efficiency with number of lines for individual dark-pulse states, that is, with a fixed detuning. Figure 7 compares the conversion efficiency for the case of a soliton microcomb and a set of different dark-pulse microcombs. The simulations use input power $P_{\text{in}} = 200$ mW, intrinsic losses $\alpha_i = 10$ dB/m, and a coupling coefficient of $\theta = 0.016$ for

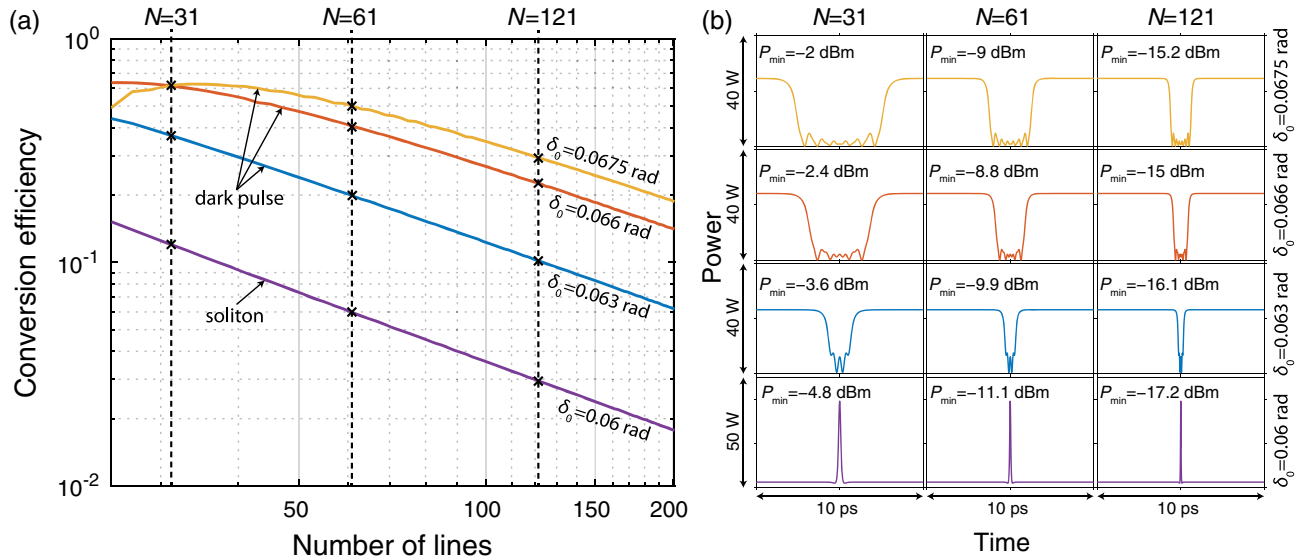

Fig. 7. Plot in (a) shows the dependence of the output conversion efficiency with the number of lines generated. The bottom curve shows the conversion efficiency of the bright soliton, while the upper curves are the conversion efficiency of dark pulses, where the different detunings correspond to different orders of dark pulses. In (b), the intracavity temporal power is plotted for the microcombs marked in (a), with the corresponding P_{min} printed above each waveform. The columns display combs with different number of lines generated, while the lines show different orders of intracavity states that correspond to the detunings in (a).

dark pulses and $\theta = 0.04$ for the dissipative Kerr soliton, which correspond to the values of the maxima observed in Fig. 2. The FSR is kept at 100 GHz, and the number of lines is adjusted by modifying the GVD value (see Fig. 6). Other parameters are the same as in Fig. 2 ($n_g = 2$ and $\gamma = 2\ \mathrm{W^{-1}\,m^{-1}}$).

The results in Fig. 7(a) reveal a clear $\sim 1/N$ scaling of the conversion efficiency with the number of lines for the soliton, as expected, but also for dark-pulse microcombs. We observed that the corresponding GVD values scaled in the same way as in Fig. 6. For further insights we provide the temporal profile for a few examples in Fig. 7(b). Clearly, the soliton pulse width decreases as the number of lines increases; since the peak power is maintained in this transition, it leads to the well-known correspondence between conversion efficiency and duty cycle [27]. The detuning in the case of the dark pulses determines the number of oscillation ripples at the bottom of the pulse. Changing the number of lines with the GVD results in a re-scaling of the waveform in an identical manner to the soliton case. This can be seen in Fig. 7(b), where the temporal characteristics become narrower with a higher number of lines. Increasing the detuning can widen the dark pulse again, which leads to an increase in conversion efficiency. However, this does not always result in an improvement of the figure of merit P_{min} (see values denoted in the figure). Optimizing P_{min} places a strong emphasis on the outer comb lines in the spectrum, which correspond to the sharp transition between high and low power amplitude with the addition of ripples on the pulse bottom. Increasing the pulse duration adds smaller ripples to the pulse, each adding a small amount of power to the outer comb lines. The interference of the oscillation leads to a highly structured pattern in the frequency domain that makes it difficult to find a direct correspondence between an optimum P_{min} and a wider dark pulse. Finally, the plateau observed around $N = 31$ corresponds to the case where the dark-pulse waveform approaches a duty cycle close to 0.5.

4. WAVEGUIDE DESIGN USING STOICHIOMETRIC SILICON NITRIDE

In the section above, narrow microcombs were proven more attractive in terms of power per line compared to broad microcombs. However, it is important to note that the design parameters of these combs can be limited in fabrication. Microresonators can be fabricated on-chip using silicon nitride for waveguides and silicon dioxide for cladding [42,47]. These materials are CMOS-compatible, and have the potential of yielding high intrinsic quality factors ($Q_i > 10^6$) [44,45] and a moderately high Kerr nonlinearity [42,48]. The coupling rate can be changed through the distance between the bus waveguide and the resonator [48,49]. The β_2 and γ can be tailored through material [42] and cross-sectional design of the waveguides [50–52]. The desired FSR is then realized by designing the length of the cavity. Since the aforementioned parameters generally display frequency dependence, each microcomb should be specifically designed for its target wavelength of operation.

Here we use a rectangular design of stoichiometric silicon nitride to evaluate if the combs presented in Fig. 6 are feasible to design. Using a commercial finite element method (FEM) solver, we find the GVD and effective nonlinear coefficient at the 1570 nm wavelength for different rectangular waveguide dimensions. The optical properties for the parameters had been retrieved through ellipsometric measurements of stoichiometric silicon nitride [43]. The results are shown as maps in Fig. 8. It is clear from the GVD map that a broad range of normal dispersive values are reachable (up to 2400 $\mathrm{ps^2/km}$), while anomalous dispersion is limited to $\beta_2 > -200\ \mathrm{ps^2/km}$.

Since narrower combs require higher dispersion values (see Fig. 6), it is evident that this platform favors dark-pulse microcombs when it comes to a narrowband superchannel design. The map of the effective nonlinear coefficient shows that all the GVD values within the range $2400\ \mathrm{ps^2/km} > \beta_2 > -200\ \mathrm{ps^2/km}$ can reach $\gamma \approx 1\ \mathrm{W^{-1}\,m^{-1}}$. To gain additional flexibility in reaching the desired GVD, more advanced designs, such as the use of concentric waveguides [50,51] or atomic layer deposition [52], appear better suited for narrowband superchannels based on soliton microcombs. It is worth noting that the performance of Turing patterns is also affected by the GVD. Bringing their line spacing to values more compatible with communications (25–100 GHz) poses challenges with regards to increasing the GVD amount [39].

Perturbations in the GVD can hinder the performance of microcombs [53]. One such perturbation is caused by mode

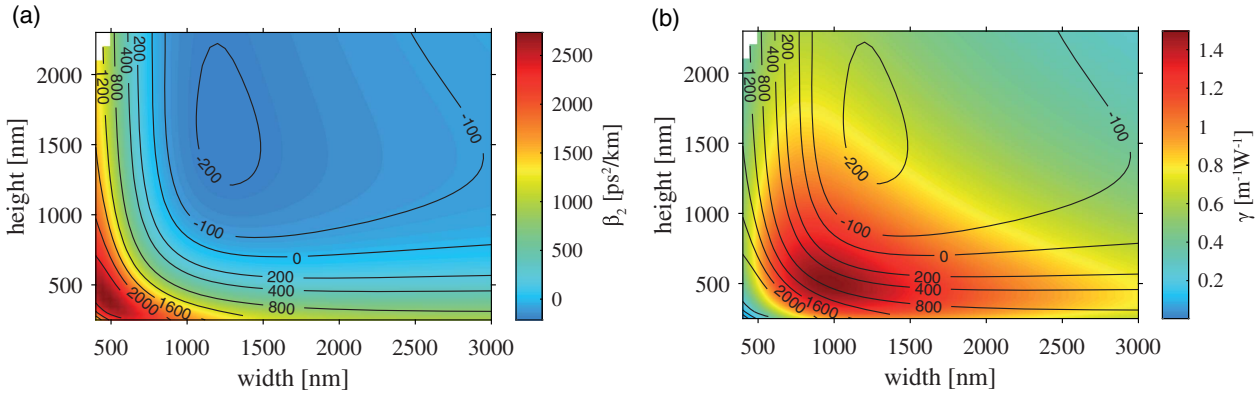

Fig. 8. Waveguide dispersion engineering (a) and the corresponding nonlinear Kerr parameter (b) for a rectangular waveguide with silicon nitride core. According to Fig. 6, this implies that the optimal narrower combs are unattainable for solitons. The right figure shows that the nonlinearities are satisfactory ($\gamma \approx 1\ \mathrm{W^{-1}\,m^{-1}}$) for most GVD values, and they can be maximized through suitable design of the cross-section geometry.

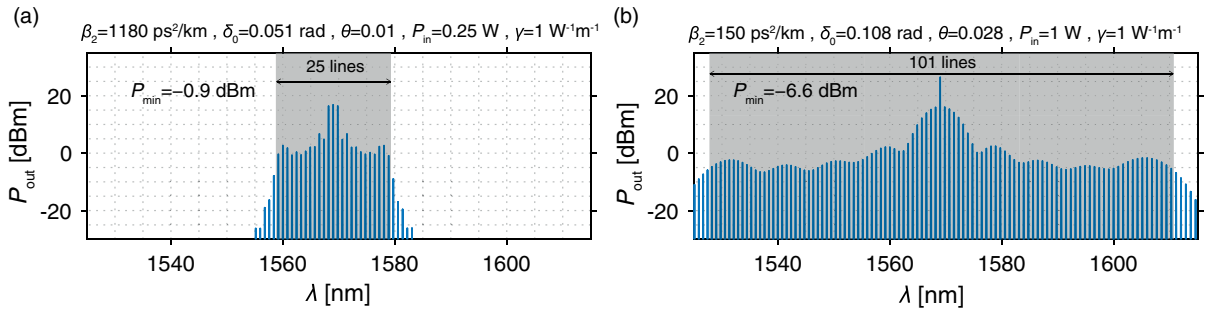

Fig. 9. The dark combs plotted here are simulated while including all higher-order dispersion determined from a geometry chosen in Fig. 8. The comb in (a) is generating 25 lines using 0.25 W input power, while the comb in (b) is generating 101 lines using 1 W of input power, where the GVD, coupling, and detuning have been optimized for $\gamma = 1\ \mathrm{W^{-1}\,m^{-1}}$. The added higher-order dispersion and the different nonlinear coefficient result in a performance drop of 1.1 dB and 1.4 dB, respectively, compared to their counterparts in Fig. 3.

coupling from different transverse modes, which can lead to diminished power in the resonances at the mode crossings. Using high-Q silicon nitride resonators will typically display decreased mode interactions [54], which reduces these effects. An alternative is to suppress the higher-order modes, e.g., by adding to the cavity an adiabatic transition to a single-mode waveguide [55].

Higher-order dispersion can affect the performance of the microcombs as well [53]. In Fig. 9, we show dark-pulse microcombs simulated with all higher-order dispersion obtained from the FEM solver for waveguide dimensions that generate the desired GVD and γ. Like the dark-pulse combs in Fig. 3, these combs have been optimized to generate 101 and 25 lines at $P_{\mathrm{in}} = 1$ W and $P_{\mathrm{in}} = 0.25$ W, respectively, but for a lower effective nonlinear coefficient $\gamma = 1\ \mathrm{W^{-1}\,m^{-1}}$. The figure shows that realistic waveguide designs, which include higher-order dispersion terms, still provide a comb line power close to the optimum design.

5. CONCLUSIONS

In summary, we have revealed that the nonlinear scaling laws for the minimum line power of soliton microcombs (similar to those in Ref. [21]) also apply for dark-pulse microcombs. The scaling suggests that for optical communications, segmenting the available bandwidth in multiple microcomb-driven superchannels is more beneficial from a power perspective. Specifically, for both dark-pulse and soliton microcombs, it shows that replacing a single comb with M superchannels increases the power per line M times, while keeping the total optical power and number of lines constant. Since the optical power of each laser providing a superchannel is relaxed, this approach is desirable for full integration.

We have shown how microcombs can be designed using rectangular silicon nitride waveguides, where narrower combs can be reached in the normal dispersive regime but are challenging to attain for soliton microcombs.

The study provides guidelines for the design of microresonator frequency combs in WDM transmission systems.

Funding. Vetenskapsrådet (VR); H2020 European Research Council (ERC) (CoG DarkComb GA 771410); National Science Foundation (NSF) (1509578-ECCS, 1809784-ECCS).

Acknowledgment. We thank Mikael Mazur and Benjamin Foo for valuable discussions when writing this paper. The simulations were performed on resources at Chalmers Centre for Computational Science and Engineering (C3SE) provided by the Swedish National Infrastructure for Computing (SNIC).

REFERENCES

1. P. Del'Haye, A. Schliesser, O. Arcizet, T. Wilken, R. Holzwarth, and T. J. Kippenberg, "Optical frequency comb generation from a monolithic microresonator," Nature **450**, 1214–1217 (2007).
2. A. M. Weiner, "Frequency combs: cavity solitons come of age," Nat. Photonics **11**, 533–535 (2017).
3. T. J. Kippenberg, R. Holzwarth, and S. A. Diddams, "Microresonator-based optical frequency combs," Science **332**, 555–559 (2011).
4. T. J. Kippenberg, A. L. Gaeta, M. Lipson, and M. L. Gorodetsky, "Dissipative Kerr solitons in optical microresonators," Science **361**, eaan8083 (2018).
5. B. Stern, X. Ji, Y. Okawachi, A. L. Gaeta, and M. Lipson, "Battery-operated integrated frequency comb generator," Nature **562**, 401–405 (2018).
6. K. A. McKinzie, C. Wang, A. A. Noman, D. L. Mathine, K. Han, D. E. Leaird, M. Anagnosti, V. Lal, G. E. Hoefler, F. Kish, M. Qi, and A. M. Weiner, "Heterogeneously integrated InP widely tunable laser and SiN microring resonator for integrated comb generation," in *Conference on Lasers and Electro-Optics*, Washington, D.C. (Optical Society of America, 2018), paper SM1B.1.
7. Y. Fan, R. M. Oldenbeuving, M. Hoekman, D. Geskus, R. Dekker, R. G. Heideman, C. G. Roeloffzen, and K.-J. Boller, "290 Hz intrinsic linewidth from an integrated optical chip-based widely tunable InP-Si3N4 hybrid laser," in *Conference on Lasers and Electro-Optics Europe & European Quantum Electronics Conference (CLEO/Europe-EQEC)* (IEEE, 2017), paper JTh5C.9.
8. A. S. Raja, A. S. Voloshin, H. Guo, S. E. Agafonova, J. Liu, A. S. Gorodnitskiy, M. Karpov, N. G. Pavlov, E. Lucas, R. R. Galiev, A. E. Shitikov, J. D. Jost, M. L. Gorodetsky, and T. J. Kippenberg, "Electrically pumped photonic integrated soliton microcomb," Nat. Commun. **10**, 680 (2019).
9. P. Del'Haye, A. Coillet, T. Fortier, K. Beha, D. C. Cole, K. Y. Yang, H. Lee, K. J. Vahala, S. B. Papp, and S. A. Diddams, "Phase-coherent microwave-to-optical link with a self-referenced microcomb," Nat. Photonics **10**, 516–520 (2016).
10. A. Fülöp, M. Mazur, A. Lorences-Riesgo, Ó. B. Helgason, P.-H. Wang, Y. Xuan, D. E. Leaird, M. Qi, P. A. Andrekson, A. M. Weiner, and V.

Torres-Company, "High-order coherent communications using mode-locked dark-pulse Kerr combs from microresonators," Nat. Commun. **9**, 1598 (2018).
11. L. Lundberg, M. Karlsson, A. Lorences-Riesgo, M. Mazur, V. Torres-Company, J. Schröder, and P. Andrekson, "Frequency comb-based WDM transmission systems enabling joint signal processing," Appl. Sci. **8**, 718 (2018).
12. V. Torres-Company, J. Schröder, A. Fülöp, M. Mazur, L. Lundberg, Ó. B. Helgason, M. Karlsson, and P. A. Andrekson, "Laser frequency combs for coherent optical communications," J. Lightwave Technol. **37**, 1663–1670 (2019).
13. J. Pfeifle, V. Brasch, M. Lauermann, Y. Yu, D. Wegner, T. Herr, K. Hartinger, P. Schindler, J. Li, D. Hillerkuss, R. Schmogrow, C. Weimann, R. Holzwarth, W. Freude, J. Leuthold, T. J. Kippenberg, and C. Koos, "Coherent terabit communications with microresonator Kerr frequency combs," Nat. Photonics **8**, 375–380 (2014).
14. J. Pfeifle, A. Coillet, R. Henriet, K. Saleh, P. Schindler, C. Weimann, W. Freude, I. V. Balakireva, L. Larger, C. Koos, and Y. K. Chembo, "Optimally coherent Kerr combs generated with crystalline whispering gallery mode resonators for ultrahigh capacity fiber communications," Phys. Rev. Lett. **114**, 093902 (2015).
15. P. Marin-Palomo, J. N. Kemal, M. Karpov, A. Kordts, J. Pfeifle, M. H. P. Pfeiffer, P. Trocha, S. Wolf, V. Brasch, M. H. Anderson, R. Rosenberger, K. Vijayan, W. Freude, T. J. Kippenberg, and C. Koos, "Microresonator-based solitons for massively parallel coherent optical communications," Nature **546**, 274–279 (2017).
16. A. Fülöp, M. Mazur, A. Lorences-Riesgo, T. A. Eriksson, P.-H. Wang, Y. Xuan, D. E. Leaird, M. Qi, P. A. Andrekson, A. M. Weiner, and V. Torres-Company, "Long-haul coherent communications using microresonator-based frequency combs," Opt. Express **25**, 26678–26688 (2017).
17. P. Liao, C. Bao, A. Kordts, M. Karpov, M. H. P. Pfeiffer, L. Zhang, A. Mohajerin-Ariaei, Y. Cao, A. Almaiman, M. Ziyadi, S. R. Wilkinson, M. Tur, T. J. Kippenberg, and A. E. Willner, "Dependence of a microresonator Kerr frequency comb on the pump linewidth," Opt. Lett. **42**, 779 (2017).
18. M. Mazur, M.-G. Suh, A. Fülöp, J. Schröder, V. Torres-Company, M. Karlsson, K. J. Vahala, and P. A. Andrekson, "Enabling high spectral efficiency coherent superchannel transmission with soliton microcombs," arXiv:1812.11046 (2018).
19. T. Herr, V. Brasch, J. D. Jost, C. Y. Wang, N. M. Kondratiev, M. L. Gorodetsky, and T. J. Kippenberg, "Temporal solitons in optical microresonators," Nat. Photonics **8**, 145–152 (2014).
20. X. Xue, Y. Xuan, Y. Liu, P.-H. Wang, S. Chen, J. Wang, D. E. Leaird, M. Qi, and A. M. Weiner, "Mode-locked dark pulse Kerr combs in normal-dispersion microresonators," Nat. Photonics **9**, 594–600 (2015).
21. C. Bao, L. Zhang, A. Matsko, Y. Yan, Z. Zhao, G. Xie, A. M. Agarwal, L. C. Kimerling, J. Michel, L. Maleki, and A. E. Willner, "Nonlinear conversion efficiency in Kerr frequency comb generation," Opt. Lett. **39**, 6126–6129 (2014).
22. S. Coen and M. Erkintalo, "Universal scaling laws of Kerr frequency combs," Opt. Lett. **38**, 1790–1792 (2013).
23. C. Godey, I. V. Balakireva, A. Coillet, and Y. K. Chembo, "Stability analysis of the spatiotemporal Lugiato-Lefever model for Kerr optical frequency combs in the anomalous and normal dispersion regimes," Phys. Rev. A **89**, 063814 (2014).
24. A. B. Matsko, A. A. Savchenkov, W. Liang, V. S. Ilchenko, D. Seidel, and L. Maleki, "Mode-locked Kerr frequency combs," Opt. Lett. **36**, 2845–2847 (2011).
25. X. Yi, Q.-F. Yang, K. Y. Yang, and K. Vahala, "Imaging soliton dynamics in optical microcavities," Nat. Commun. **9**, 3565 (2018).
26. H. Guo, M. Karpov, E. Lucas, A. Kordts, M. H. P. Pfeiffer, V. Brasch, G. Lihachev, V. E. Lobanov, M. L. Gorodetsky, and T. J. Kippenberg, "Universal dynamics and deterministic switching of dissipative Kerr solitons in optical microresonators," Nat. Phys. **13**, 94–102 (2017).
27. X. Xue, P.-H. Wang, Y. Xuan, M. Qi, and A. M. Weiner, "Microresonator Kerr frequency combs with high conversion efficiency," Laser Photon. Rev. **11**, 1600276 (2017).
28. A. B. Matsko, A. A. Savchenkov, and L. Maleki, "Normal group-velocity dispersion Kerr frequency comb," Opt. Lett. **37**, 43–45 (2012).
29. W. Liang, A. A. Savchenkov, V. S. Ilchenko, D. Eliyahu, D. Seidel, A. B. Matsko, and L. Maleki, "Generation of a coherent near-infrared Kerr frequency comb in a monolithic microresonator with normal GVD," Opt. Lett. **39**, 2920–2923 (2014).
30. V. Lobanov, G. Lihachev, T. J. Kippenberg, and M. Gorodetsky, "Frequency combs and platicons in optical microresonators with normal GVD," Opt. Express **23**, 7713–7721 (2015).
31. P. Parra-Rivas, E. Knobloch, D. Gomila, and L. Gelens, "Dark solitons in the Lugiato-Lefever equation with normal dispersion," Phys. Rev. A **93**, 063839 (2016).
32. S. Wabnitz, "Suppression of interactions in a phase-locked soliton optical memory," Opt. Lett. **18**, 601–603 (1993).
33. P. Parra-Rivas, D. Gomila, E. Knobloch, S. Coen, and L. Gelens, "Origin and stability of dark pulse Kerr combs in normal dispersion resonators," Opt. Lett. **41**, 2402–2405 (2016).
34. S. Chandrasekhar and X. Liu, "Advances in Tb/s superchannels," in *Optical Fiber Telecommunications VIB*, I. P. Kaminow, T. Li, and A. E. Willner, eds., 6th ed. (Academic, 2013), chap. 3.
35. X. Liu, S. Chandrasekhar, and P. J. Winzer, "Digital signal processing techniques enabling multi-Tb/s superchannel transmission: an overview of recent advances in DSP-enabled superchannels," IEEE Signal Process. Mag. **31**(2), 16–24 (2014).
36. Ó. B. Helgason, A. Fülöp, J. Schröder, P. A. Andrekson, and A. M. Weiner, "Superchannel engineering with microresonator combs," in *Conference on Lasers and Electro-Optics* (2018), paper JW2A.71.
37. L. Lundberg, E. Borjeson, C. Fougstedt, M. Mazur, M. Karlsson, P. A. Andrekson, and P. Larsson-Edefors, "Power consumption savings through joint carrier recovery for spectral and spatial superchannels," in *European Conference on Optical Communication (ECOC)* (2018), paper We2.26.
38. D. C. Cole, E. S. Lamb, P. Del'Haye, S. A. Diddams, and S. B. Papp, "Soliton crystals in Kerr resonators," Nat. Photonics **11**, 671–676 (2017).
39. V. Torres-Company, D. Castelló-Lurbe, and E. Silvestre, "Comparative analysis of spectral coherence in microresonator frequency combs," Opt. Express **22**, 4678–4691 (2014).
40. K. Ikeda, "Multiple-valued stationary state and its instability of the transmitted light by a ring cavity system," Opt. Commun. **30**, 257–261 (1979).
41. J. M. Dudley and S. Coen, "Coherence properties of supercontinuum spectra generated in photonic crystal and tapered optical fibers," Opt. Lett. **27**, 1180–1182 (2002).
42. D. J. Moss, R. Morandotti, A. L. Gaeta, and M. Lipson, "New CMOS-compatible platforms based on silicon nitride and Hydex for nonlinear optics," Nat. Photonics **7**, 597–607 (2013).
43. C. J. Krückel, A. Fülöp, Z. Ye, P. A. Andrekson, and V. Torres-Company, "Optical bandgap engineering in nonlinear silicon nitride waveguides," Opt. Express **25**, 15370–15380 (2017).
44. Y. Xuan, Y. Liu, L. T. Varghese, A. J. Metcalf, X. Xue, P.-H. Wang, K. Han, J. A. Jaramillo-Villegas, A. Al Noman, C. Wang, S. Kim, M. Teng, Y. J. Lee, B. Niu, L. Fan, J. Wang, D. E. Leaird, A. M. Weiner, and M. Qi, "High-Q silicon nitride microresonators exhibiting low-power frequency comb initiation," Optica **3**, 1171–1180 (2016).
45. M. H. P. Pfeiffer, J. Liu, A. S. Raja, T. Morais, B. Ghadiani, and T. J. Kippenberg, "Ultra-smooth silicon nitride waveguides based on the damascene reflow process: fabrication and loss origins," Optica **5**, 884–892 (2018).
46. S. Coen, H. G. Randle, T. Sylvestre, and M. Erkintalo, "Modeling of octave-spanning Kerr frequency combs using a generalized mean-field Lugiato-Lefever model," Opt. Lett. **38**, 37 (2013).
47. J. S. Levy, A. Gondarenko, M. A. Foster, A. C. Turner-Foster, A. L. Gaeta, and M. Lipson, "CMOS-compatible multiple-wavelength oscillator for on-chip optical interconnects," Nat. Photonics **4**, 37–40 (2010).
48. M. H. P. Pfeiffer, J. Liu, M. Geiselmann, and T. J. Kippenberg, "Coupling ideality of integrated planar high-Q microresonators," Phys. Rev. Appl. **7**, 024026 (2017).

49. W.-P. Huang, "Coupled-mode theory for optical waveguides: an overview," J. Opt. Soc. Am. A **11**, 963–983 (1994).
50. M. Soltani, A. Matsko, and L. Maleki, "Enabling arbitrary wavelength frequency combs on chip," Laser Photon. Rev. **10**, 158–162 (2016).
51. S. Kim, K. Han, C. Wang, J. A. Jaramillo-Villegas, X. Xue, C. Bao, Y. Xuan, D. E. Leaird, A. M. Weiner, and M. Qi, "Dispersion engineering and frequency comb generation in thin silicon nitride concentric microresonators," Nat. Commun. **8**, 372 (2017).
52. J. Riemensberger, K. Hartinger, T. Herr, V. Brasch, R. Holzwarth, and T. J. Kippenberg, "Dispersion engineering of thick high-Q silicon nitride ring-resonators via atomic layer deposition," Opt. Express **20**, 27661–27669 (2012).
53. T. Herr, V. Brasch, J. D. Jost, I. Mirgorodskiy, G. Lihachev, M. L. Gorodetsky, and T. J. Kippenberg, "Mode spectrum and temporal soliton formation in optical microresonators," Phys. Rev. Lett. **113**, 123901 (2014).
54. J. Liu, A. S. Raja, M. Karpov, B. Ghadiani, M. H. P. Pfeiffer, B. Du, N. J. Engelsen, H. Guo, M. Zervas, and T. J. Kippenberg, "Ultralow-power chip-based soliton microcombs for photonic integration," Optica **5**, 1347–1353 (2018).
55. A. Kordts, M. H. P. Pfeiffer, H. Guo, V. Brasch, and T. J. Kippenberg, "Higher order mode suppression in high-Q anomalous dispersion SiN microresonators for temporal dissipative Kerr soliton formation," Opt. Lett. **41**, 452–455 (2016).